Proceedings of ASME Turbo Expo 2025
Turbomachinery Technical Conference and Exposition
GT2025
June 16-20, 2025, Memphis, Tennessee

GT2025-152711

OXIDATION OF AN ENVIRONMENTAL BARRIER COATED CERAMIC MATRIX COMPOSITE IN A COMBUSTION ENVIRONMENT

Michael J. Presby
NASA Glenn Research Center
Cleveland, OH, USA

Roy M. Sullivan
NASA Glenn Research Center
Cleveland, OH, USA

Leland C. Hoffman
HX-5, LLC
Cleveland, OH, USA

Bryan J. Harder
NASA Glenn Research Center
Cleveland, OH, USA

Kang N. Lee
NASA Glenn Research Center
Cleveland, OH, USA

ABSTRACT

Oxidation is a key failure mechanism for environmental barrier coatings (EBCs) deposited on ceramic matrix composites (CMCs). Current generation EBC/CMC systems incorporate a silicon (Si) bond coat between the CMC substrate and the EBC topcoat. Oxidation occurs at the interface between the Si bond coat and the EBC topcoat due to diffusion of water vapor and oxygen creating a thermally grown silica (SiO_2) scale. As the SiO_2 scale increases in thickness, the adhesion strength of the EBC topcoat becomes compromised leading to delamination and spallation. This work investigates the oxidation kinetics of an EBC/CMC system with an Si bond coat utilizing a natural gas/oxygen (NG/O_2) burner rig at atmospheric pressure. An oxidation model is presented to predict the oxidation kinetics of the EBC/CMC system. The model exhibits good agreement with experimental data obtained in the NG/O_2 rig up to 250 hours after which the oxidation kinetics deviate from the predicted behavior. A reason for the observed change in oxidation kinetics is presented along with directions for future work.

Keywords: Environmental barrier coatings (EBCs); ceramic matrix composites (CMCs); oxidation; burner rig.

1. INTRODUCTION

Ceramic matrix composites (CMCs) have proven to be an important material technology for gas turbine engine manufacturers in the pursuit of developing more efficient engines [1-3]. The best-performing CMCs are produced with silicon carbide fibers embedded in a silicon carbide matrix, or SiC/SiC CMCs. These materials have a low density, approximately one-third that of nickel-based superalloys, and exhibit excellent mechanical properties (strength, toughness) at elevated temperatures [4]. However, SiC-based materials have a vulnerability to water vapor. In a gas turbine engine, water vapor is generated as a by-product of combustion. SiC reacts with oxidizing species such as oxygen (O_2) and water (H_2O) at high temperatures and results in the formation of a silica (SiO_2) oxide scale. The SiO_2 scale further reacts with water vapor in the combustion environment to form a gaseous silicon hydroxide species, $Si(OH)_4$, resulting in material loss [5]. This material loss, termed recession, leads to reduced structural integrity of the material, and significantly limits the life of SiC/SiC CMCs making them unsuitable for use in gas turbine engines. To mitigate this issue and improve the durability of SiC/SiC CMCs, environmental barrier coatings (EBCs) were developed [5]. Simply, EBCs act as a barrier to the combustion environment, preventing recession of the underlying CMC.

Current, state-of-the-art EBCs incorporate a silicon (Si) bond coat between the CMC substrate and EBC topcoat as displayed in the schematic of Figure 1. The EBC topcoat consists of rare-earth (RE) silicates with the general formula of RE_2SiO_5 (RE monosilicate) or $RE_2Si_2O_7$ (RE disilicate). The Si bond coat is incorporated to aid adhesion between the substrate and EBC topcoat and to protect the substrate from oxidation.

While EBCs provide a barrier to SiC recession, the EBC topcoat can also react with water vapor at high temperature [5]; however, these reactions occur at a slow, acceptable rate. In addition, EBCs are not a diffusion barrier, so water vapor and oxygen still permeate through the EBC topcoat. This leads to oxidation of the Si bond coat resulting in the formation of a thermally grown oxide (TGO) scale of SiO_2 between the Si bond coat and the EBC topcoat [5]. Oxidation of the Si bond coat is a key failure mechanism for EBCs because once the TGO scale reaches a critical thickness, the EBC topcoat will delaminate and spall, leaving no protective barrier from the combustion environment which results in rapid material loss. As a result, it is important to understand the oxidation kinetics of EBC/CMC

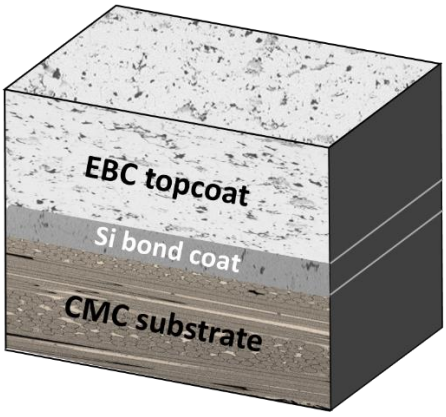

FIGURE 1: EBC/CMC system: CMC substrate, Si bond coat and EBC topcoat. The EBC topcoat can be single or multi-layered.

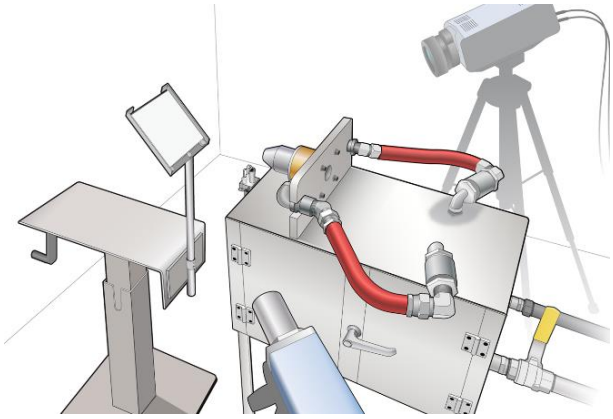

FIGURE 2: Burner rig platform and EBC/CMC test coupon.

systems to accurately model and predict material and component lifetimes.

In this work, the oxidation kinetics of an EBC/CMC system are investigated in a combustion environment using a natural gas/oxygen (NG/O_2) burner rig [6]. An oxidation model is presented to predict the TGO thickness and compared to the experimental results.

2. MATERIALS AND METHODS

2.1 Materials

The EBC/CMC system investigated in this work consisted of a 2D woven (0/90°), melt-infiltrated (MI) SiC/SiC CMC. The CMC contained Hi-Nicalon™ Type S (HNS) fibers with a boron nitride (BN) interphase [7]. The CMC panel consisted of eight plies with a total, average thickness of 3.05 mm. Three CMC coupons were then fabricated from the panel with dimensions (length by width) of 76.2 mm by 76.2 mm. The bulk density of the CMC was determined to be 2.58 ± 0.06 g/cm^3.

The EBC system was deposited onto the CMC coupons via air plasma spray (APS). The deposition was performed after the CMC coupons were cut to size (76.2 mm by 76.2 mm) and grit blasted with cubic boron nitride. A Si bond coat was deposited to a nominal thickness of 127 μm followed by a nominally 254 μm thick ytterbium disilicate ($Yb_2Si_2O_7$) topcoat. The EBC was applied to one surface of the CMC coupon. The total thickness of each coupon (EBC + CMC) was approximately 3.43 mm. Each sample was tested in the as-deposited condition with no post-deposition heat treatment or annealing step performed.

2.2 Methods

An atmospheric natural gas/oxygen (NG/O_2) burner rig was used to expose the EBC/CMC coupons to a combustion environment. The NG/O_2 burner rig was described in detail elsewhere [6] but will be discussed here briefly.

A schematic of the NG/O_2 burner rig test set-up is shown in Figure 2. The burner platform consists of a 19.05 mm surface mixing nozzle and a dual electrode pilot to ignite the flame. In parallel to a continuous supply of natural gas, an oxygen system generates high purity oxygen (~93%) and supplies it to the rig enabling continuous operation. The supply of natural gas and oxygen can be adjusted via two mass flow controllers to deliver up to 700 standard cubic feet per hour (SCFH) of natural gas and up to 1500 SCFH oxygen. Wonderware Historian is used for data acquisition, data storage, and monitoring the status of the rig.

The test coupons were held at a 45° angle with respect to the burner nozzle using an Inconel fixture with the EBC surface in direct impingement of the flame. The distance from the nozzle exit to the center of the sample was approximately 15.24 cm. The EBC surface temperature was monitored with a long wavelength infrared (LWIR) pyrometer (Williamson Corp., Concord, MA USA) and a thermal imaging camera (Teledyne FLIR, Wilsonville, OR USA). The spectral ranges for both the pyrometer and thermal imaging camera are approximately 10.1 to 11 μm. The pyrometer and thermal imaging camera require knowledge of the sample emittance for accurate temperature measurements. The high temperature spectral emittance of the $Yb_2Si_2O_7$ EBC was measured and reported elsewhere [8]. Based on the spectral response of the pyrometer and thermal imaging camera, a weighted average high temperature emittance for the $Yb_2Si_2O_7$ EBC was determined to be 0.92. The CMC backside surface temperature was monitored with a dual-wavelength IR pyrometer (Williamson Corp., Concord, MA USA) with spectral bands at 0.8 and 0.9 μm.

Three tests were performed with durations of 25, 250, and 500 hours at an EBC surface temperature of 1482°C and CMC backside temperature of ~1200°C. The NG flow rate was set to 100 SCFH and the O_2 flow rate was set to 650 SCFH to reach the target EBC temperature. At the time of testing, automatic thermal cycling capability was not available in the burner rig so the test campaign was performed by heating the samples up to temperature and holding for the given duration (25, 250, and 500 hours). However, the two longer duration tests (250 and 500 hours) required periodic shutdowns at approximately 100-hour intervals to clean the nozzle of carbon buildup, so some thermal cycling still occurred. In addition, based on the thermal conductivity and thicknesses of the various layers in the system, the temperature at the $Yb_2Si_2O_7$ EBC topcoat and Si bond coat interface was estimated to be approximately 1316°C.

Post-testing, the samples were cut, mounted in epoxy, and polished for analysis using scanning electron microscopy (SEM), and wavelength dispersive spectroscopy (WDS).

3. OXIDATION MODEL

The framework for modeling oxidation of the EBC/CMC system comes from the formulation by Deal and Grove [9] for the oxidation of Si. The Deal and Grove model was revisited in 2019 by Sullivan [10] to include the effects of a protective coating layer (e.g., EBC). A detailed analysis of this reformulation can be found in the work by Sullivan [10], but an overview will be presented here, briefly. A schematic of the problem being modeled is shown in Figure 3.

The reformulation of the linear-parabolic equation to account for an EBC assumes that oxidants diffuse across the topcoat of thickness, δ, from the surrounding gas environment as the molecules O_2 and H_2O. These molecules react and oxidize the Si bond coat to form a thermally grown oxide (TGO) layer of SiO_2 with thickness, x_o. For continuous growth of TGO, the oxidants must then diffuse across both the topcoat and TGO layers. Under steady-state conditions, the oxidant concentration is linear within the EBC and TGO layers. The oxidant concentration at the exterior surface of the EBC is denoted as C_o while the equilibrium concentration C^* is the oxidant concentration at the outer surface that is in equilibrium with the partial pressure of the oxidant in the gas environment, P. The equilibrium concentration, C^*, can be expressed as a function of P using Henry's law: $C^* = H_c P$ where H_c is the solubility coefficient for the oxidant in the EBC. The oxidant concentration is discontinuous at the topcoat/SiO_2 interface where C_a^c is the concentration in the topcoat, and C_a^o is the concentration in the TGO. The concentration at the TGO/Si interface is denoted as C_i.

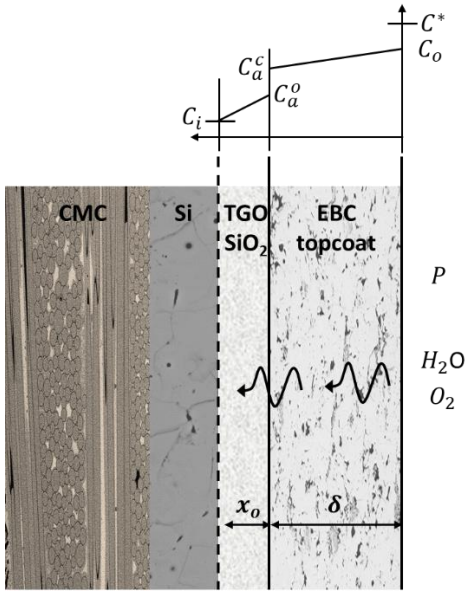

FIGURE 3: EBC/CMC system consisting of an Si bond coat and EBC topcoat, with a TGO layer (SiO_2) between them. P is the oxidant partial pressure (H_2O or O_2) in the gas environment, C^* is the equilibrium oxidant concentration at the outer surface that is in equilibrium with the partial pressure of the oxidant, C_o is the oxidant concentration at the exterior surface of the EBC topcoat, C_a^c is the oxidant concentration in the EBC topcoat at the topcoat/TGO interface, C_a^o is the oxidant concentration in the TGO at the topcoat/TGO interface, C_i is the oxidant concentration at the TGO/Si interface, δ is the topcoat thickness, and x_o is the TGO thickness.

The oxidant in the topcoat and TGO at the interface is assumed to be in equilibrium with the oxidant in a theoretical gas reservoir at an oxidant partial pressure, P^a. As such, $C_a^c = H_c P^a$ and $C_a^o = H_{TGO} P^a$, where H_{TGO} is the solubility coefficient for the oxidant in the TGO. Introducing $\bar{H} = H_c / H_{TGO}$, one can rewrite $C_a^c = \bar{H} C_a^o$. It is worth noting in Figure 3 that $C_a^c > C_a^o$, but this may not always be the case as C_a^c and C_a^o depend on the values of H_c and H_{TGO}, respectively.

Based on the formulation of Deal and Grove [9] and Sullivan [10], the steady-state fluxes are

$$F_1 = h(C^* - C_o) \tag{1a}$$

$$F_2 = D_c \frac{(C_o - C_a^c)}{\delta} = D_c \frac{(C_o - \bar{H} C_a^o)}{\delta} \tag{1b}$$

$$F_3 = D_{TGO} \frac{(C_a^o - C_i)}{x_o} \tag{1c}$$

$$F_4 = k C_i \tag{1d}$$

where h relates the flux of oxidant from the gas environment to the topcoat surface, D_c is the diffusivity of the topcoat, D_{TGO} is the diffusivity of the TGO layer, and k is a reaction rate constant.

Under steady-state conditions, $F_1 = F_2 = F_3 = F_4$. This leads to an expression for the oxidant flux, F:

$$F = F_1 = F_2 = F_3 = F_4 = \frac{kC^*}{\frac{k}{h} + \bar{H}\left(1 + \frac{k x_o}{D_{TGO}}\right) + \frac{k\delta}{D_c}} \tag{2}$$

The rate of increase of the SiO_2 thickness and the oxidant flux are related by:

$$\frac{dx_o}{dt} = \frac{F}{N} \tag{3}$$

where N is the number of oxidant molecules in a unit volume of SiO_2. Assuming $h \gg k$ and provided $\bar{H}$ is not a small number, substituting Equation (2) into Equation (3), integrating, and simplifying yields the following expression:

$$x_o^2 + A' x_o = B(t + \tau) \tag{4}$$

where

$$A' = \frac{2D_{TGO}}{k} + \frac{2D_{TGO}}{\bar{H}D_c}\delta \quad (5)$$

$$B = \frac{2D_{TGO}}{N} H_{TGO} P \quad (6)$$

$$\tau = \frac{x_{o,i}^2 + A' x_{o,i}}{B} \quad (7)$$

and $x_{o,i}$ is the initial thickness of TGO. It is worth noting that the relationships given by Equations (5) and (6) for A' and B, respectively, can also be expressed in terms of permeability, γ where $\gamma = HD$.

Despite the significance for development and modeling of EBC systems, O_2 and H_2O diffusivity or permeability data is extremely limited. Measurements of O_2 permeability through rare earth silicates has been reported by Wada et. al. [11], but measurements for the permeability of water appear to be unavailable. Nevertheless, estimates for A' and B can be obtained by fitting Equation (4) to TGO thickness versus time measurement data obtained from air (21% O_2 + ~79% N_2) and steam (90% H_2O + 10% O_2) oxidation testing which are readily available.

For the identical EBC system used in this work (Si/$Yb_2Si_2O_7$), and the same layer thicknesses (Si: 127 μm and $Yb_2Si_2O_7$: 254 μm) air and steam oxidation data at atmospheric pressure has been reported previously at 1316°C [12]. These tests were performed on a chemical vapor infiltrated (CVI) SiC/SiC CMC substrate. It's worth noting that the steam oxidation tests were performed cyclically with one hour hot (1316°C), and 20 minutes cool (<100°C) [12]. The air and cyclic steam oxidation data from this study are shown graphically in Figure 4.

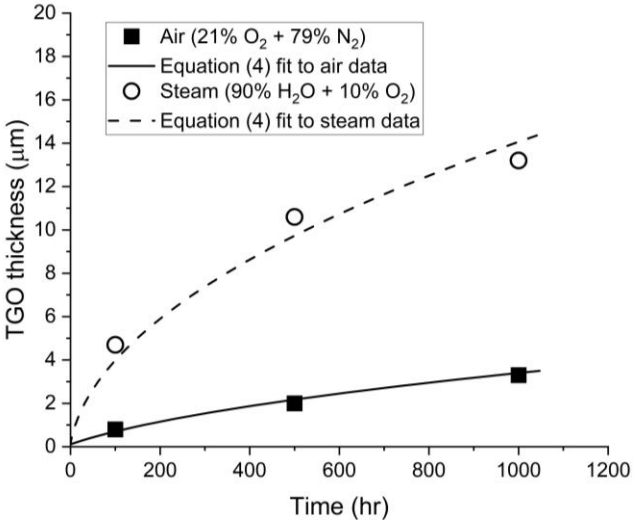

FIGURE 4: TGO thickness versus time for Si/$Yb_2Si_2O_7$ EBC oxidation at 1316°C in air, and steam. Data extracted from [12]. Note: chemical vapor infiltrated (CVI) SiC/SiC CMC substrate.

TABLE 1: Rate constants for oxidation of Si/$Yb_2Si_2O_7$ EBC determined via regression analysis of experimental data for air and cyclic steam oxidation at atmospheric pressure.

	A' (μm)	B (μm²/hr)	τ (hr)
Air (21% O_2 + 79% N_2)	2.57	0.02	14.96
Steam[a] (90% H_2O + 10% O_2)	1.6	0.22	1.25

[a] Optimization performed with constraint $A' \geq 1.6$ [13].

A regression analysis can be performed to obtain the best fit of Equation (4) to the experimental data. The best-fit values for A', B, and τ are displayed in Table 1 and the corresponding curves are also included in Figure 4. The linear-parabolic model represented by Equation (4) along with the rate constants shown in Table 1 can be used to predict the TGO thickness as a function of time for the Si/$Yb_2Si_2O_7$ EBC in the NG/O_2 combustion environment.

The NG and O_2 flow rates of 100 SCFH and 650 SCFH, respectively, corresponds to an equivalence ratio, ϕ ~ 0.33. Utilizing NASA's Chemical Equilibrium with Applications (CEA) code [14], the mole fractions of O_2 and H_2O – the primary gas species responsible for oxidation – can be calculated. The calculated mole fractions are 0.512 for O_2 and 0.238 for H_2O. These values are also equal to the partial pressures of O_2 and H_2O since the NG/O_2 burner is at atmospheric pressure. Based on the calculated mole fractions, the NG/O_2 rig is a combined environment where O_2 and H_2O will contribute to the overall oxidation rate. Therefore, the rate of oxidation in the NG/O_2 rig will be the summation of the rate of oxidation due to O_2 and the rate of oxidation due to H_2O. Based on the relationship given by Equation (4), the total rate of oxidation is given by:

$$\frac{dx_o}{dt} = \frac{B_{(O_2)}}{A'_{(O_2)} + 2x_o} + \frac{B_{(H_2O)}}{A'_{(H_2O)} + 2x_o} \quad (8)$$

The values of A' shown in Table 1 are directly applicable for O_2 and H_2O where $A'_{(O_2)}$ = 2.57 and $A'_{(H_2O)}$ = 1.6. The constant B, however, is linearly dependent upon the partial pressure, P of the oxidant as expressed by Equation (6). As a result, the values for B in Table 1 need to be adjusted based on the partial pressure of the oxidants in the NG/O_2 combustion environment. This leads to $B_{(O_2)} = \frac{0.02}{0.21}(0.512) = 0.049$ and $B_{(H_2O)} = 0.22(0.238) = 0.052$. For purposes of calculating $B_{(H_2O)}$, it is assumed that the value obtained in Table 1 for 90% H_2O + 10% O_2 is approximately equal to that for 100% H_2O. It should be noted that the rate constants in Table 1 are from air and cyclic steam oxidation testing at 1316°C (no thermal gradient) while EBC/CMC testing in the NG/O_2 rig is performed with a thermal gradient with the EBC surface at 1482°C and CMC back surface at 1200°C. However, the NG/O_2 test was conducted such that the temperature at the Si bond coat (e.g., the location where oxidation will take place) would be approximately 1316°C based on the thickness and thermal conductivity of the EBC. Therefore, it is assumed that the rate constants obtained under oxidation in

air and steam are applicable to the burner rig tests. Also, the burner rig samples experienced some cycling which allowed for the β-α phase transformation of the TGO, particularly for the longer duration tests. As such, the difference in cycle frequency between the burner rig and cyclic steam oxidation tests is assumed to be negligible. However, further work is certainly merited to understand the effects of thermal gradients and cycle frequency on oxidation and diffusion to verify these assumptions.

Using the rate constants for the NG/O_2 environment, Equation (8) can be numerically solved for TGO thickness versus time using a time-stepping approach where:

$$x_o^t = x_o^{t-1} + \frac{dx_o}{dt}\Delta t \qquad (9)$$

The predicted TGO thickness versus time for the Si/$Yb_2Si_2O_7$ EBC in the NG/O_2 environment for ϕ = 0.33 is shown in Figure 5. For the experimental test durations of 25, 250 and 500 hours, the predicted TGO thicknesses are approximately 0.89, 4.12, and 6.17 μm, respectively.

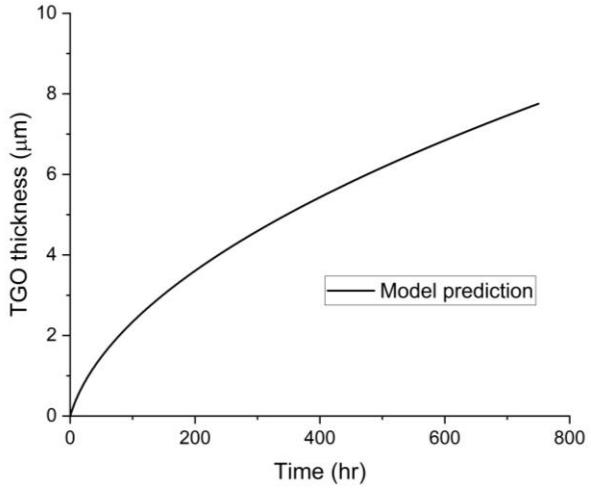

FIGURE 5: Predicted TGO thickness versus time for the Si/$Yb_2Si_2O_7$ EBC system in the NG/O_2 environment.

4. EXPERIMENTAL RESULTS AND DISCUSSION

Representative SEM cross-sections for the three test durations (25, 250, and 500 hours) are shown in Figure 6. The SEM images were taken at the center of each sample which is aligned with the central region of the flame. The average TGO thickness and standard deviation were determined via image analysis [15] and are displayed in Table 2. These measurements are shown graphically in Figure 7 along with the model prediction.

The experimental data is in good agreement with the model prediction up to 250 hours. At 500 hours, the experimental data deviates from the predicted linear-parabolic behavior where the TGO thickness at 500 hours is approximately 1.7 times greater than the predicted thickness. Damage to the EBC (e.g., cracking

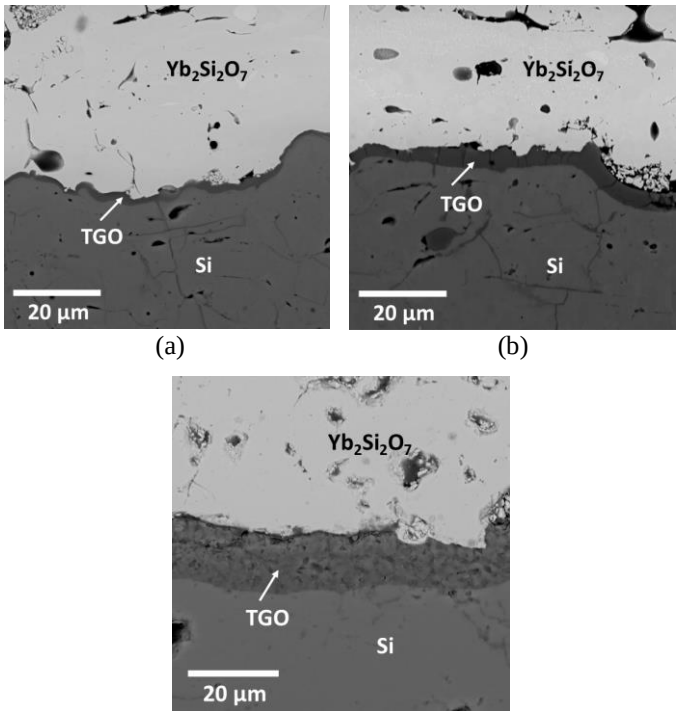

FIGURE 6: Representative SEM cross-sections showing the TGO thickness after (a) 25 hours, (b) 250 hours, and (c) 500 hours.

TABLE 2: Experimental TGO thickness measurements.

Test Duration (hr)	Average thickness (μm)	Standard Deviation (μm)
25	1.32	0.39
250	4.32	1.18
500	10.58	1.24

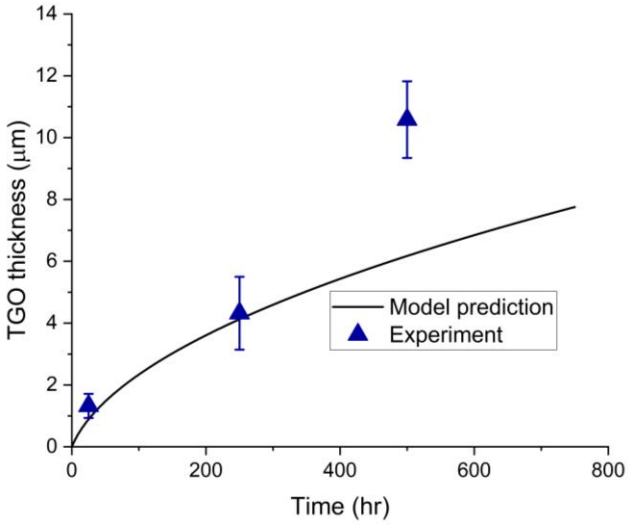

FIGURE 7: Experimental results for TGO thickness compared to the model prediction.

or spallation) could result in higher oxidation rates due to the rapid ingress of combustion gases; however, no apparent damage distress, nor recession/erosion of the EBC was observed in the 500-hour sample. It's worth noting that a crack was observed in the 250-hour sample, but it occurred outside the area of interest and is not expected to have influenced the TGO thickness measured at the center of the sample.

With the absence of damage to the EBC in the 500-hour sample, deviation from the expected linear-parabolic behavior could be a result of increased oxidation due to substrate chemistry effects. Lee [16] highlighted the effect of substrate chemistry on the oxidation of EBCs where it was shown that an accelerated oxidation rate was directly related to the substrate boron content. Substrates with higher boron content may exhibit greater oxidation rates due to boron readily diffusing through the Si bond coat. Other studies have also reported that boron increases the oxidation rates of both Si and SiC [17-18].

For SiC/SiC CMCs, the SiC fibers are coated with boron nitride (BN) to facilitate fiber/matrix debonding. In CVI SiC/SiC CMCs, boron is only present in the BN fiber coating while the matrix is boron free. For MI SiC/SiC CMCs, the MI process can require additions of boron to the matrix slurry to ensure wetting and complete melt penetration of the fiber preform [16, 19-20].

Lee [16] compared the oxidation rate on CVI and MI SiC/SiC substrates and found that boron readily diffuses through the Si bond coat for the EBC deposited on the MI substrate. Boron was detected in the TGO via wavelength dispersion spectroscopy (WDS). For the EBC deposited on a CVI substrate, no boron was detected in the TGO. This resulted in thicker TGO scales on the MI substrate compared to the CVI substrate.

To further investigate this phenomenon, WDS (Advanced Microbeam, Inc. Vienna, OH USA) was also performed on the burner rig samples. Boron was not readily detected in the Si bond coat nor the TGO for the 25- and 250-hour samples. This correlates well with the experimental data and oxidation model where both the 25- and 250-hour data points were in good agreement with the prediction (see Fig. 7). For the 500-hour sample, boron was readily detected in the TGO with levels ranging between 0.24 and 2.5 wt.%. This correlates with the results reported by Lee [16] and with the deviation of the 500-hour sample from the predicted behavior.

To further investigate this phenomenon, we revisit the results reported by Lee [16] for the cyclic steam oxidation testing (90% H_2O + 10% O_2) on the MI SiC/SiC CMC. The results reported by Lee [16] were on the exact EBC/CMC system used in this study. Figure 8 shows the experimental data for cyclic steam oxidation compared to predicted behavior. The 500- and 1000-hour data were extracted from [16] and the 100- and 300-hour data were added in this work to better highlight the trend. Similar to the burner rig data, it is evident that the oxidation rate for the cyclic steam oxidation breaks away from the predicted linear-parabolic behavior. In addition, the oxidation rate for the cyclic steam oxidation data appears to exhibit behavior that is more linear with time.

Recall that the rate constants used for the model predictions were obtained from data reported on the Si/$Yb_2Si_2O_7$ EBC deposited on a CVI SiC/SiC CMC [12], so the prediction in Figure 8 for cyclic steam oxidation is essentially the best fit of the data presented in Figure 4. However, since the rate constants used in the model represent that of the EBC system deposited on a CVI substrate, it is believed that these constants represent the oxidation of the EBC system without any substrate effects due to boron. Nonetheless, boron is a common additive for MI CMCs that appears to play a significant role in the overall oxidation behavior. As such, there is a need to develop a fundamental understanding of the effects of boron diffusion on the oxidation of this system.

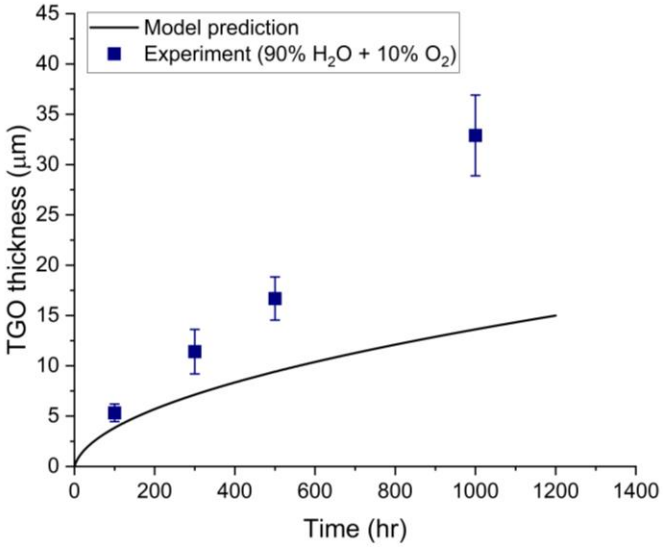

FIGURE 8: Experimental results for the cyclic steam oxidation (90% H_2O + 10% O_2) for the Si/$Yb_2Si_2O_7$ EBC on MI SiC/SiC compared to the model prediction. The 500 and 1000-hour data were extracted from [16] while the 100 and 300-hour data were added in this work.

5. MODEL REFORMULATION AND DISCUSSION

We revisit the modeling framework in attempt to understand the effects of boron diffusion on the observed oxidation kinetics. In the reformulation, we now consider boron diffusing into the Si bond coat from the CMC substrate as shown schematically in Figure 9. Initially, no boron is present in the Si bond coat and an initial TGO (TGO 1) is formed with diffusivity, D_1. At time t_b, boron arrives at the oxidation site and a subsequent TGO layer (TGO 2) is formed with diffusivity D_2. The thickness of TGO 1 is denoted as x_{o1} and the thickness of TGO 2 is denoted as x_{o2}. The steady-state fluxes are:

$$F_1 = h(C^* - C_o) \tag{10a}$$

$$F_2 = D_c \frac{(C_o - C_a^c)}{\delta} = D_c \frac{(C_o - \bar{H} C_a^o)}{\delta} \tag{10b}$$

$$F_3 = D_1 \frac{(C_a^o - C_b)}{x_{o1}} \tag{10c}$$

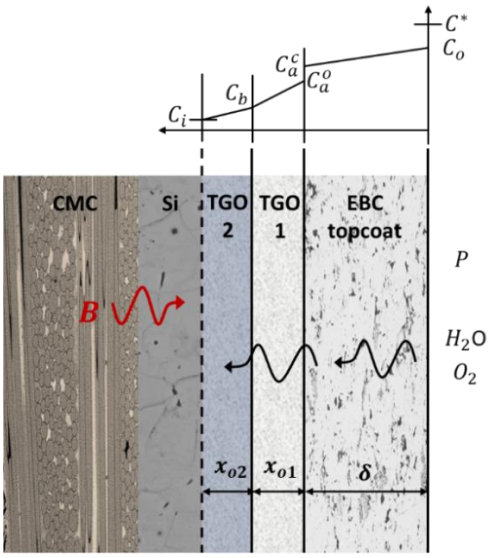

FIGURE 9: Reformulated EBC/CMC system considering boron diffusing from the substrate through the Si bond coat and the formation of TGO 1 when no boron is present in the Si bond coat at the oxidation site, and the formation of TGO 2 when boron is present at the oxidation site.

$$F_4 = D_2 \frac{(C_b - C_i)}{x_{o2}} \tag{10d}$$

$$F_5 = kC_i \tag{10e}$$

Equating all the fluxes leads to a new linear-parabolic equation represented by the relationship of Equation (4) with new expressions for A' and B (denoted as A'_2 and B_2) where:

$$A'_2 = \frac{D_2}{D_1}(A'_1 + 2x_{o1}) \tag{11}$$

$$B_2 = \frac{D_2}{D_1} B_1 \tag{12}$$

and A'_1 and B_1 are given by Equations (5) and (6), respectively. The rate of change of TGO 1 $\left(\frac{dx_{o1}}{dt}\right)$ is still governed by Equation (8) while the rate of change of TGO 2 is governed by:

$$\frac{dx_{o2}}{dt} = \frac{B_{2(O_2)}}{A'_{2(O_2)} + 2x_{o2}} + \frac{B_{2(H_2O)}}{A'_{2(H_2O)} + 2x_{o2}} \tag{13}$$

The total rate of change of the TGO will now be governed by the following:

$$\frac{dx_o}{dt} = \frac{dx_{o1}}{dt} + \frac{dx_{o2}}{dt} \tag{14}$$

where

$$\frac{dx_{o1}}{dt} = 0 \text{ for } t \geq t_b \tag{15}$$

and

$$\frac{dx_{o2}}{dt} = 0 \text{ for } t < t_b. \tag{16}$$

Equations (8) and (13) are solved numerically via the time-stepping approach. For $t \geq t_b$ the total TGO thickness is the sum of the final thickness of TGO 1 and the thickness of TGO 2.

A parametric study can be performed to understand the effects of the diffusivity ratio, $\frac{D_2}{D_1}$ and the boron arrival time, t_b on the TGO growth behavior.

Figure 10 shows the results for $\frac{D_2}{D_1}$ = 10 and $\frac{D_2}{D_1}$ = 100 and boron arrival times (t_b) ranging from 25 to 200 hours as compared to the original prediction and NG/O_2 experimental data. For a diffusivity ratio of 10 (Figure 10a), linear-parabolic behavior is observed, and the model suggests that boron needs to start arriving at the oxidation site between 25 and 50 hours to best match the experimental data out to 500 hours. As the diffusivity ratio increases to 100 (Figure 10b), the boron arrival time required to best fit the experimental data is 50 hours, and the curves become linear.

We now investigate the effect of changing the diffusivity ratio while holding the boron arrival time fixed at 50 hours since this time appears to provide the best match with the experimental data. Figure 11 shows the result of increasing the diffusivity ratio from 10 to 1000. The results shown in Figure 11 suggest that a diffusivity ratio of at least 50 would be required to best model the experimental data out to 500 hours. In other words, the diffusivity of TGO 2 would need to be at least 50 times greater than the diffusivity of TGO 1.

The change in behavior from linear-parabolic to linear as the diffusivity ratio increases can be reasoned from the relationships given by Equations (11) and (13). When $\frac{D_2}{D_1}$ becomes large, then $A'_2 \gg 2x_{o2}$ and it follows that $\frac{dx_{o2}}{dt}$ would be approximately constant. This corresponds to a linear TGO growth rate. As $\frac{D_2}{D_1}$ becomes large, TGO 2 effectively provides zero resistance to diffusion of the oxidants. Therefore, as $\frac{D_2}{D_1} \to \infty$, then:

$$\frac{dx_{o2}}{dt} = \frac{B_{1(O_2)}}{A'_{1(O_2)} + 2x_{o1}} + \frac{B_{1(H_2O)}}{A'_{1(H_2O)} + 2x_{o1}} \tag{16}$$

From Equation (16), it is evident that the growth rate of TGO 2 is governed by the rate of diffusion through the EBC topcoat and TGO 1 when the diffusivity ratio becomes large. Therefore, it follows that the TGO thickness is bounded by the line given as:

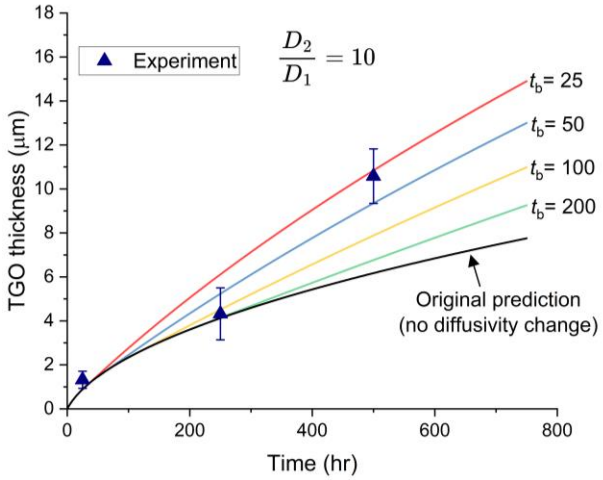

(a)

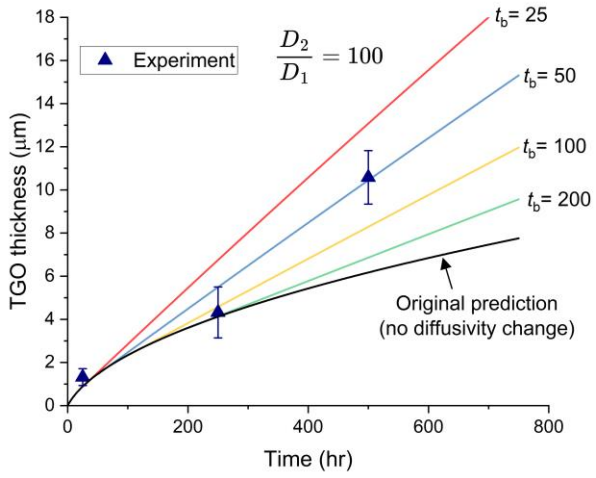

(b)

FIGURE 10: TGO thickness versus time curves compared to the experimental NG/O_2 burner rig data for (a) $\frac{D_2}{D_1}$ = 10, and (b) $\frac{D_2}{D_1}$ = 100 and boron arrival times, t_b ranging from 25 to 200 hours.

$$x_o = \frac{B_{1(O_2)}}{A'_{1(O_2)} + 2x_{o1f}}(t - t_b) + \frac{B_{1(H_2O)}}{A'_{1(H_2O)} + 2x_{o1f}}(t - t_b) + x_{o1f} \quad (17)$$

where x_{o1f} is the final thickness of TGO 1 which occurs at the boron arrival time, t_b. This is shown graphically by the dashed line in Figure 12.

The reformulated model framework is now applied to the cyclic steam oxidation data and is shown in Figure 13 for a boron arrival time of 50 hours and the diffusivity ratio varying from 10 to 1000. It's evident that the model reformulation also fits the cyclic steam oxidation data for a diffusivity ratio of 50 or greater. This ultimately suggests that similar behavior is observed for the

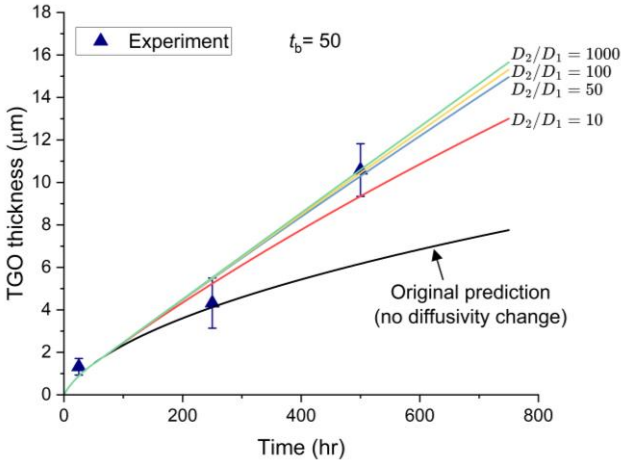

FIGURE 11: TGO thickness versus time curves compared to the experimental NG/O_2 burner rig data for a boron arrival time, t_b = 50 hours and diffusivity ratio, $\frac{D_2}{D_1}$ ranging from 10 to 1000.

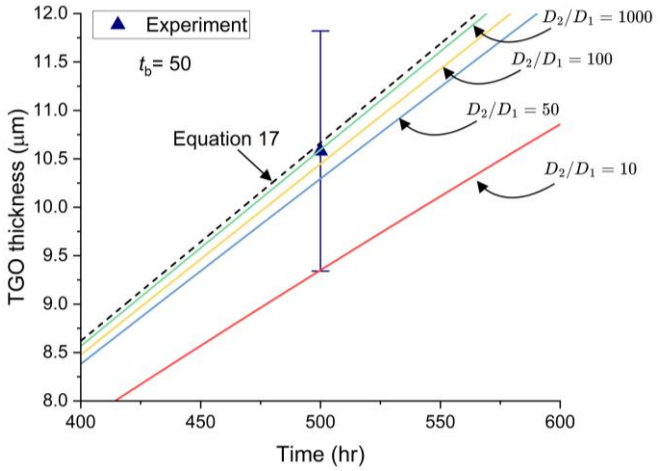

FIGURE 12: TGO thickness versus time curves (t_b = 50 hours, and $\frac{D_2}{D_1}$ ranging from 10 to 1000) approaching the line represented by Equation 17 as $\frac{D_2}{D_1}$ increases.

EBC/CMC system in the NG/O_2 burner rig and the cyclic steam oxidation tests when accounting for differences in the partial pressure of the oxidants. However, the cyclic steam oxidation data appears to exhibit linear behavior that is in better agreement with the reformulated model compared to the burner rig data. This could be a result of the steam oxidation testing being performed in a controlled environment with no thermal gradients compared to the dynamic combustion environment with a thermal gradient in the burner rig. Diffusion of boron may occur more readily through the thickness of the CMC in the steam oxidation environment since the entire substrate is at 1316°C versus the burner rig test where substrate temperature varies from ~1316°C at the EBC/substrate interface to ~1200°C at the backside of the sample. Additionally, the effect of thermal cycling, particularly in the steam oxidation rigs, could also play

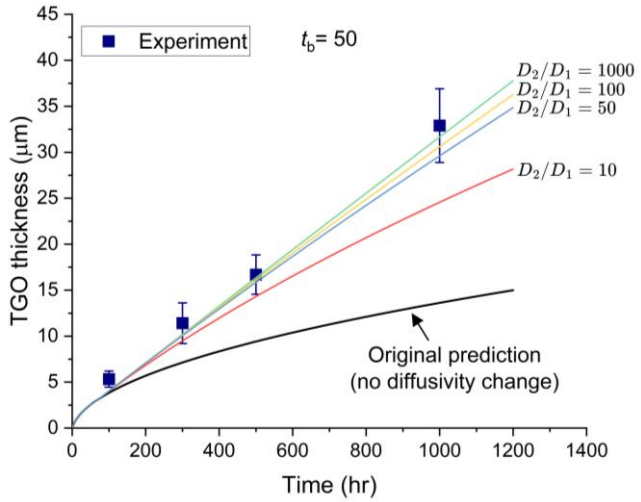

FIGURE 13: TGO thickness versus time curves compared to the experimental cyclic steam oxidation data for a boron arrival time, t_b = 50 hours and diffusivity ratio, $\frac{D_2}{D_1}$ ranging from 10 to 1000.

a role in the observed behavior. Nonetheless, the reformulation appears to model the oxidation rate of the EBC/CMC system reasonably well. Nevertheless, several key items related to the rate constants used in the model, substrate chemistry, boron arrival time, and the diffusivity ratio need to be addressed.

First, it must be re-emphasized that the rate constants used in the model were extracted from experimental oxidation data in air and steam. This was performed due to the lack of measured values for the diffusivity/permeability of EBC constituents. To fully understand the oxidation behavior of the EBC/CMC system and validate the modeling framework, future efforts to obtain measured values for the diffusivity/permeability of EBC constituents is warranted.

Second, the effects of substrate chemistry on the oxidation behavior of EBC/CMC systems cannot be overlooked. As shown in this work and previous work [16], boron from the substrate can diffuse through the Si bond coat leading to accelerated oxidation which ultimately has significant implications for the long-term durability of EBC/CMC systems in the gas turbine environment. Based on the model reformulation, it is predicted that boron arrives at the oxidation site around 50 hours to match the experimental results. To investigate if it is feasible for boron to diffuse across the Si bond coat in 50 hours, we formulate a 1-D diffusion model. For 1-D diffusion in a semi-infinite medium, $x > 0$, where the boundary is kept at a constant concentration, C_s with a constant diffusivity, D, the governing partial differential equation is [21]:

$$\frac{\partial C}{\partial t} - D\frac{\partial^2 C}{\partial x^2} = 0 \qquad (18)$$

Equation (18) is subject to the boundary condition $C(0,t) = C_s$ and the initial condition $C(x,0) = 0$. The solution to Equation (18) that satisfies the boundary condition and initial condition is:

$$C(x,t) = C_s erfc\left(\frac{x}{2\sqrt{Dt}}\right) \qquad (19)$$

where $erfc$ is the complementary error function. The diffusivity, D of boron in silicon has been reported previously up to 1342°C [22]. At 1316°C, the interface temperature of the Si bond coat in this work, $D \approx 1 \times 10^{-11}$cm^2/s [22]. Figure 14a shows the normalized boron concentration as a function of distance for $D = 1 \times 10^{-11}$cm^2/s where it would take approximately 300 hours for boron to start arriving at the oxidation site. For boron to arrive at the oxidation site in 50 hours, the diffusivity of boron in the Si bond coat would need to be at least an order of magnitude faster. As shown in Figure 14b, a small concentration of boron would be expected at the oxidation site at 50 hours for $D = 1 \times 10^{-10}$ cm^2/s. The diffusivity reported in [22] is for boron diffusing

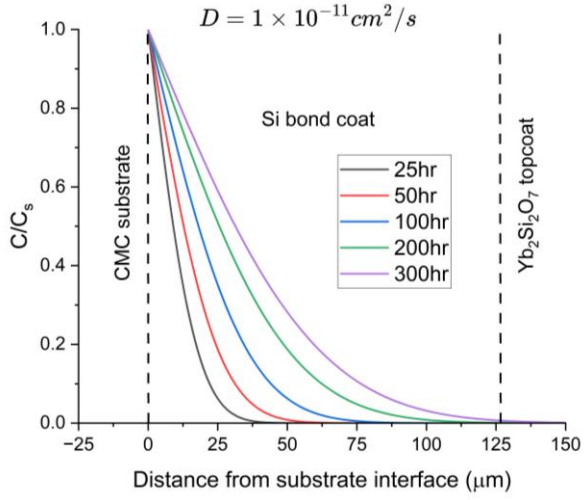

(a)

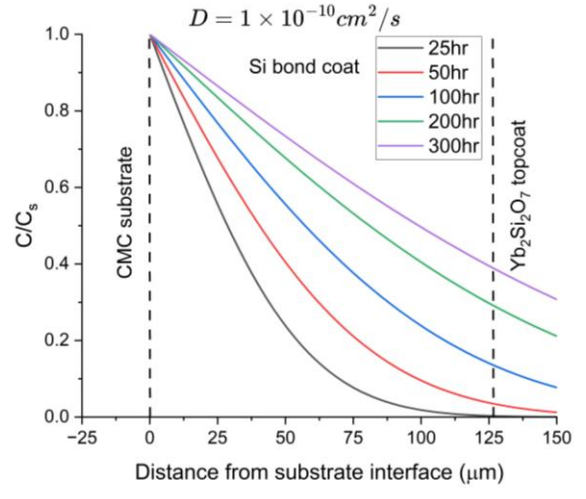

(b)

FIGURE 14: Results of a 1-D diffusion model for boron through the Si bond coat (a) $D = 1 \times 10^{-11}$ cm^2/s, and (b) $D = 1 \times 10^{-10}$ cm^2/s.

through single crystal, *n*-type Si, and it is likely that the diffusivity of boron in APS Si, which contains higher porosity levels, would have a higher diffusivity. However, diffusivity measurements of boron into APS Si are not currently available and further work in this area is required. In addition to measuring the diffusivity of boron into the APS Si bond coat, a question that arises is what concentration of boron would be required at the oxidation site to begin generating a TGO with higher diffusivity?

Lastly, the modeling framework is based on the growth of two separate, distinct TGOs. The diffusivity of TGO 2, which forms after boron arrives at the oxidation site, would need to be at least 50 times greater than TGO 1, which originally forms with boron not being present at the oxidation site. Additional work is required to understand this proposed oxidation mechanism, and to understand the chemical composition and crystal structure of the TGO before and after boron arrives at the oxidation site. Previous work on oxygen diffusion of boron doped Si [17] suggested that boron probably produces defects in the SiO_2 lattice which results in a structure that provides an increase in diffusion. It is worth noting that the diffusion of oxygen through different silicate glasses has been reported and can vary by orders of magnitude [23-24]. Therefore, efforts to directly measure TGO diffusivities are required to fully comprehend the observed behavior and to validate the modeling framework. Nonetheless, this first approach to model the oxidation of the burner rig and cyclic steam oxidation data has provided some valuable insight into additional areas to explore.

6. CONCLUSION

The oxidation behavior of a silicon/ytterbium disilicate ($Si/Yb_2Si_2O_7$) EBC system deposited onto an MI SiC/SiC CMC was investigated in a natural gas/oxygen combustion environment. An oxidation model was developed based on a modified Deal and Grove theory to include the EBC system. The experimental data was in good agreement with the model up to 250 hours after which the oxidation behavior deviated from the expected linear-parabolic behavior. The deviation was attributed to the diffusion of boron from the MI SiC/SiC CMC substrate that accelerated oxidation. The presence of boron was detected in the TGO via WDS analysis, and the results were consistent with previously reported results from cyclic steam oxidation. The oxidation model was reformulated to account for the diffusion of boron and the formation of a TGO layer with modified diffusivity. A parametric study showed that the model could predict the experimental behavior reasonably well. However, experimental measurements for diffusivity and permeability are unknown and are required to validate the model.

ACKNOWLEDGEMENTS

This work was supported by the Commercial Supersonic Technology (CST) and Hybrid Thermally Efficient Core (HyTEC) projects at NASA Glenn Research Center. The authors would also like to thank Don Lesher at Advanced Microbeam for performing the WDS analysis.

REFERENCES

[1] Fellet, M., 2015, Ceramic-matrix composites take the heat, *MRS Bull.*, 40, pp. 916-917.

[2] Steibel, J., 2019, Ceramic matrix composites taking flight at GE Aviation, *Am. Ceram. Soc. Bull.*, 98, 3, pp. 30-33.

[3] Bouillon, E.P., Ojard, G.C., Habarou, G., Spriet, P.C., Lecordix, J.L., Feindel, D.T., Linsey, G.D., Stetson, D.P., 2022, Characterization and nozzle test experience of a self-sealing ceramic matrix composite for gas turbine applications, *Proc. ASME Turbo 2022: Power for Land, Sea, and Air. Vol. 4*., Amsterdam, The Netherlands, June 3-6, 2002, pp. 15-21.

[4] Zok, F.W., 2016, Ceramic-matrix composites enable revolutionary gains in turbine engine efficiency, *Am. Ceram. Soc. Bull.*, 95, 5, pp. 22-28.

[5] Lee, K.N., Zhu, D., Lima, R.S., 2021, Perspectives on environmental barrier coatings (EBCs) manufactured via air plasma spray (APS) on ceramic matrix composites (CMCs): a tutorial paper, *J. Therm. Spray Tech.*, 30, pp. 40-58.

[6] Presby, M.J., Endo, M., Fox, D.S., Harder, B.J., Lee, K.N., Hoffman, L.C., Cuy, M.D., 2024, The development and use of a natural gas/oxygen burner rig for environmental barrier coating and ceramic matrix composite technology maturation, *ASME J. Eng. Gas Turbines Power*, 146, 1, pp. 011012-1 – 011012-11.

[7] Presby, M.J., 2021, High-temperature solid particle erosion in a melt-infiltrated SiC/SiC ceramic matrix composite, *ASME J. Eng. Gas Turbines Power*, 143, 12, pp. 121026-1 – 121026-6.

[8] Presby, M.J., Crowell, S.F., Eldridge, J.I., Markham, J.R., 2024, Spectral emittance measurements for ytterbium disilicate-based environmental barrier coatings, *Intl. J. Ceram. Eng. Sci.*, 6, 5, pp. 1-11.

[9] Deal, B.E., Grove, A.S., 1965, General relationship for the thermal oxidation of silicon, *J. Appl. Phys.*, 36, 12, pp. 3770-3778.

[10] Sullivan, R.M., 2019, Reformulation of oxide growth equations for oxidation of silicon bond coat in environmental barrier coating systems, *J. Euro. Ceram. Soc.*, 39, 16, pp. 5403-5409.

[11] Wada, M., Matsudaira, T., Kawashima, N., Kitaoka, S., Takata, M., 2017, Mass transfer in polycrystalline ytterbium disilicate under oxygen potential gradients at high temperatures, *Acta Mater.*, 135, pp. 372-381.

[12] Lee, K.N., 2019, $Yb_2Si_2O_7$ environmental barrier coatings with reduced bond coat oxidation rates via chemical modifications for long life, *J. Am. Ceram. Soc.*, 102, pp. 1507-1521.

[13] Sullivan, R.M., Stuckner, J., Lee, K.N., Jaskowiak, M.H., 2023, Estimates of permeability of water vapor in rare earth silicate environmental barrier coatings using the modified theory of Deal and Grove, *Ceram. Intl.*, 49, 11 Part A, pp. 18014-18018.

[14] McBride, B.J., Sanford, G., 1996, Computer program for calculations of complex chemical equilibrium compositions and applications II. User's manual and program description, *National Aeronautics and Space Administration*, Report No. 19950013764.

[15] Stuckner, J., Harder, B., Smith, T.M., 2022, Microstructure segmentation with deep learning encoders pre-trained on a large microscopy dataset, *npj Comput. Mater.*, 8, 200.

[16] Lee, K.N., Garg, A., Jennings, W.D., 2021, Effects of the chemistry of coating and substrate on the steam oxidation kinetics of environmental barrier coatings for ceramic matrix composites, *J. Eur. Ceram. Soc.*, 41, pp. 5675 – 5685.

[17] Deal, B.E., Sklar, M., 1965, Thermal Oxidation of Heavily Doped Silicon, *J. Electrochem. Soc.*, 112, 430.

[18] McFarland, B., Opila, E.J., 2018, Silicon carbide fiber oxidation behavior in the presence of boron nitride, *J. Am. Ceram. Soc.*, 101, pp. 5534-5551.

[19] Gray, P., 2006, Method for performing silicon melt infiltration of ceramic matrix composites, *U.S. Patent Application*, 11/039,814.

[20] Shim, S., Shinavski, R, 2020, Reducing surface nodules in melt-infiltrated ceramic matrix composites, *U.S. Patent*, 10,822,279.

[21] Crank, J., 1979, The mathematics of diffusion, *Oxford Univ. Press*.

[22] Kurtz, A.D., Yee, R., 1960, Diffusion of boron into silicon, *J. Appl. Phys.*, 31, pp. 303-305.

[23] Sucov, E.W., 1963, Diffusion of oxygen in vitreous silica, *J. Am. Ceram. Soc.*, 46, 1, pp. 14-20.

[24] Doremus, R.H., 1962, Diffusion in non-crystalline silicates, *Modern Aspects of the Vitreous State*, Vol. 2, Ed. MacKenzie, J.D., Butterworth and Co. Ltd., London, pp.1-71.